A Fast Registration Method Combining Self-Adaptive Segmentation Model and NDT for MEMS LiDAR Point Cloud

Xuemei Li *, Bin Liu , Shangsong Lv , Min Li , Chengjie Liu

Posted Date: 30 June 2023

doi: 10.20944/preprints202306.2176.v1

Keywords: Intelligent information perception; point cloud registration; vehicle mounted MEMS LiDAR; SSM-NDT algorithm; self-adaptive segmentation model; autonomous vehicle

Article

A Fast Registration Method Combining Self-Adaptive Segmentation Model and NDT for MEMS LiDAR Point Cloud

Xuemei Li[1*], Bin Liu[2], Shangsong Lv[2], Min Li[2], Chengjie Liu[2]

[1] College of Mechanical and Control Engineering, Baicheng Normal University, Baicheng 137000, China; Liubinwork666@163.com (B.L.)
[2] College of Information and Control Engineering, Jilin Institute of Chemical Technology, Jilin 132022, China; 1916409631@qq.com (S.L.); 2053587656@qq.com (M.L); 1455485812@qq.com (C.L.)
* Correspondence: lixuemei556677@163.com

Abstract: The Micro-Electro-Mechanical System (MEMS) LiDAR point cloud in autonomous vehicles has a large deflection range, which results in slow registration speed and poor applicability. To maximize speed, an improved NDT (Normal Distribution Transform) method that integrates point cloud density features has been proposed. First, the point cloud is reduced using a modified voxel filter and a pass-through filter. Next, the ISS (Intrinsic Shape Signature) algorithm is utilized to analyze the point cloud features and extract keypoints, the 4PCS (4-Point Congruent Sets) algorithm is then employed to calculate the initial pose under the constraints of the keypoint set to complete the coarse registration. Finally, the self-adaptive segmentation model is constructed by using KD-tree to obtain the density features of keypoints, and the NDT algorithm is combined with this model to form an SSM-NDT algorithm, which is used for fine registration. Each algorithm was compared on the autonomous vehicle dataset PandaSet and actual collected data sets, the results show that the novel method increases the speed by at least 60% and takes into account good registration accuracy and strong anti-interference.

Keywords: Intelligent information perception; point cloud registration; vehicle mounted MEMS LiDAR; SSM-NDT algorithm; self-adaptive segmentation model; autonomous vehicle

1. Introduction

As one of the sensors of autonomous vehicles' environment perception, LiDAR is regarded as the "eye" with its advantages of high resolution, strong anti-interference ability, and high stability. MEMS LiDAR has promising technological development prospects due to its miniaturization, low power consumption, and low cost, and gradually becoming one of the main sensors for autonomous vehicles. As the vehicle moves, the LiDAR captures point cloud information from different perspectives of the target. Therefore, it is necessary to concatenate the front and rear frames to obtain the target's complete 3D point cloud information [1].

Point cloud registration refers to matching and aligning source and target point clouds to maximize their overlap. Its core is to solve the spatial rotation and translation matrix between the source and target point cloud [2]. Besl [3] proposed a groundbreaking Iterative Closest Point (ICP) algorithm, The ICP has high registration accuracy but has harsh application conditions. Therefore, scholars from various countries had proposed a series of improved algorithms [4–10].

In addition to ICP, Magnusson [11] proposed the NDT algorithm. Aiger [12] proposed the 4PCS algorithm. Theiler [13] proposed the K4PCS algorithm, which first extracts key points using the 3D-Harris [14] or 3D-DoG [15] algorithms. Xu [16] proposed a 4-Plane Congruent Set based on Voxel geometric constraint (V4PCS) algorithm for semi-automatic.

When point cloud data (PCD) have massive information, the feature-based coarse registration method is usually used. This method can only select special points for registration without the need for the initial pose, including feature description and extraction. Commonly used feature descriptors

Preprints (www.preprints.org) | NOT PEER-REVIEWED | Posted: 30 June 2023 doi:10.20944/preprints202306.2176.v1

include PFH, FPFH, SHOT, 3DSC, CSF, RMF, 2D Line Features, and LPPF [17–23]; Keypoint extraction algorithms include 3D DoG, 3D Harris, SIFT, Hough Transform, and RANSAC based plane detection [24–26].

In recent years, new methods have been constantly emerging, and application scenes have been expanding [27–34]. Among them, an improved ICP algorithm combining RANSAC, ISS, and 3DSC is proposed in [30]. In [31], point features are extracted by calculating the FPFH, and RANSAC and ICP are used to search and align.

In outdoor environments, MEMS LiDAR may collect PCD with high noise and low overlap due to frequent changes in road conditions and vehicle speeds. Proposed a fast registration method for this. The method takes preprocessing, coarse registration, and fine registration as the main axis, and combined them with an improved voxel filter, keypoints extraction, and self-adaptive segmentation model (SSM). The effectiveness of the method on the PandaSet [35] and The Real LiDAR-Derived PCD is verified. Compared with other algorithms, the new method is precise and efficient.

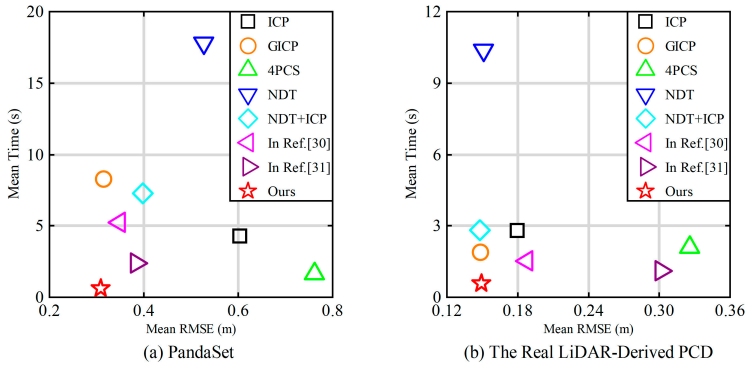

Figure 1. Accuracy and runtime (The mean root mean square error (RMSE) and mean Time of different registration algorithms in PandaSet and The Real LiDAR-Derived PCD).

The remainder of this paper is as organized follows. Section 2 provides the registration process and characteristics of the 4PCS and NDT algorithms. Section 3 introduces the proposed algorithm's registration strategy, principle, and partial program flow. Next, the comparison results between our method and existing algorithms are presented in Section 4. Finally, Section 5 introduces the conclusions and future work.

2. Related Works

2.1. 4PCS Algorithm

The 4PCS algorithm utilizes the principle of affine invariance to search for approximately identical coplanar 4-point sets in two frames and determines the optimal transformation matrix T_{best} by calculating the degree of overlap.

Randomly select three points a, b, and c to determine a plane, then select a point d to form the plane $B \subset P$. Let the line ac intersect the line bd at point e, as shown in Figure 2:

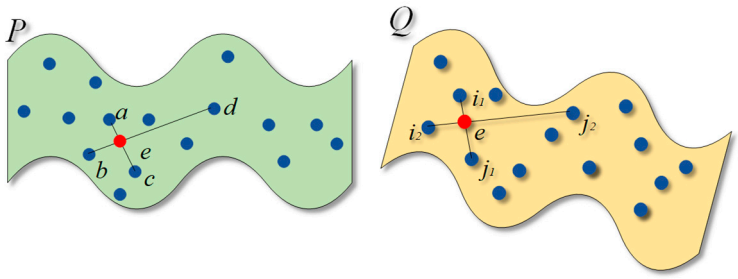

Figure 2. Collect and pair a 4-point set.

So, obtain two affine invariant ratios R_1 and R_2:

Preprints (www.preprints.org) | NOT PEER-REVIEWED | Posted: 30 June 2023 doi:10.20944/preprints202306.2176.v1

$$R_1 = {||a-e_1||}/{||a-c||}, \; R_2 = {||b-e_1||}/{||b-d||} \tag{1}$$

For any point-pair $i_1, j_1 \in Q$, calculate two intersections that conform to the affine ratio:

$$e_1 = i_1 + R_1 (j_1 - i_1), \; e_2 = i_1 + R_2 (j_1 - i_1) \tag{2}$$

During the pairing process, approximately coplanar point sets are often used for matching, so it is necessary to eliminate point sets with significant differences.

If Q is transformed by T_k to Q', and the distance between any point in Q' and any point in P is d, then:

$$d = ||q_{Q'} - q_P|| < \varepsilon \tag{3}$$

Where: $q_{Q'}$, q_P are any points in Q' and P, respectively, ε is the distance threshold of point-pairs.

If point cloud P and Q are in ε the set of 4-point sets paired within the range is $D = \{D_1, ..., D_k\}$, calculate T_k between the plane pairs B, U within D. Allocate matching scores based on the number of point-pairs that comply with equation (3). When the score is the highest, $T_{best} = T_k$.

To use 4PCS, three important parameters need to be provided: ε, the approximate overlap rate O_r, and the target distance D_t. Compared to ICP, 4PCS does not require initial pose, has good anti-interference and a wide range of applications, and is usually used for coarse registration.

2.1. NDT Algorithm

Magnusson was inspired by the 2D-NDT [36] algorithm and expanded from 2D to 3D. Its core is to establish a continuous and differentiable probability density function (PDF) based on the normal distribution of 3D density. Thus, the solution of the transformation matrix is transformed into the optimization of continuous function. The schematic is shown in Figure 3.

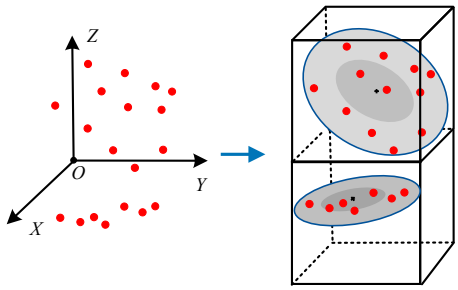

Figure 3. Shape features and NDT representation.

The steps of the NDT algorithm are as follows:

Step 1: Divide the space into blocks and place the target point cloud into blocks.

Step 2: Calculate the parameters, mean vector $\vec{\mu}$ and covariance matrix Σ of the PDF, whose values are:

$$\vec{\mu} = \frac{1}{m}\sum_{k=1}^{m} \vec{y_k}, \; \Sigma = \frac{1}{m}\sum_{k=1}^{m} (\vec{y_k} - \vec{\mu})(\vec{y_k} - \vec{\mu})^T \tag{4}$$

Where: m is the number of points within a block; $\vec{y_k}$ is the scanning points of the target point cloud within the block; T is the transformation matrix.

Step 3: Initialize or update the transformation parameters and search for the corresponding block again.

Step 4: Calculate the PDF of the block:

$$f(\vec{x}) = {Exp\left(-\frac{1}{2}\Sigma^{-1}(\vec{x}-\vec{\mu})(\vec{x}-\vec{\mu})^T\right)}\Big/{(2\pi)^{\frac{D}{2}}\sqrt{|\Sigma|}} \tag{5}$$

Where: $D = 3$; $\vec{x}$ is a Scan point within the source cloud.

Step 5: To obtain the optimal transformation matrix, maximize the likelihood function:

$$\Theta = \prod_{k=1}^{n} f(T(\vec{p}, \vec{x_k})) \tag{6}$$

Preprints (www.preprints.org) | NOT PEER-REVIEWED | Posted: 30 June 2023 doi:10.20944/preprints202306.2176.v1

Where: $T(\vec{p},\vec{x_k})$ represents transforming $\vec{x_k}$ through $\vec{p}$.

Minimize the objective function $F(\vec{p})$, which is the negative logarithm of the likelihood function.

$$F(\vec{p}) = -log\Theta = -\sum_{i=1}^{n} log f(T(\vec{p},\vec{x_k})) \quad (7)$$

Step 6: Establish the score function g_{score}, use the Newton algorithm to minimize the g_{score}, and update the transformation.

Step 7: Finally, determine whether the updated amount is converging. If so, end. Otherwise, repeat steps 3 to 6.

NDT divides point cloud space into multiple small blocks for statistical calculation, which enables it to quickly process large-scale PCD and to some extent overcome the influence of noise and outliers.

3. Methodology

The method includes three parts: Preprocessing, Coarse registration, and Fine registration. See Figure 3 for details.

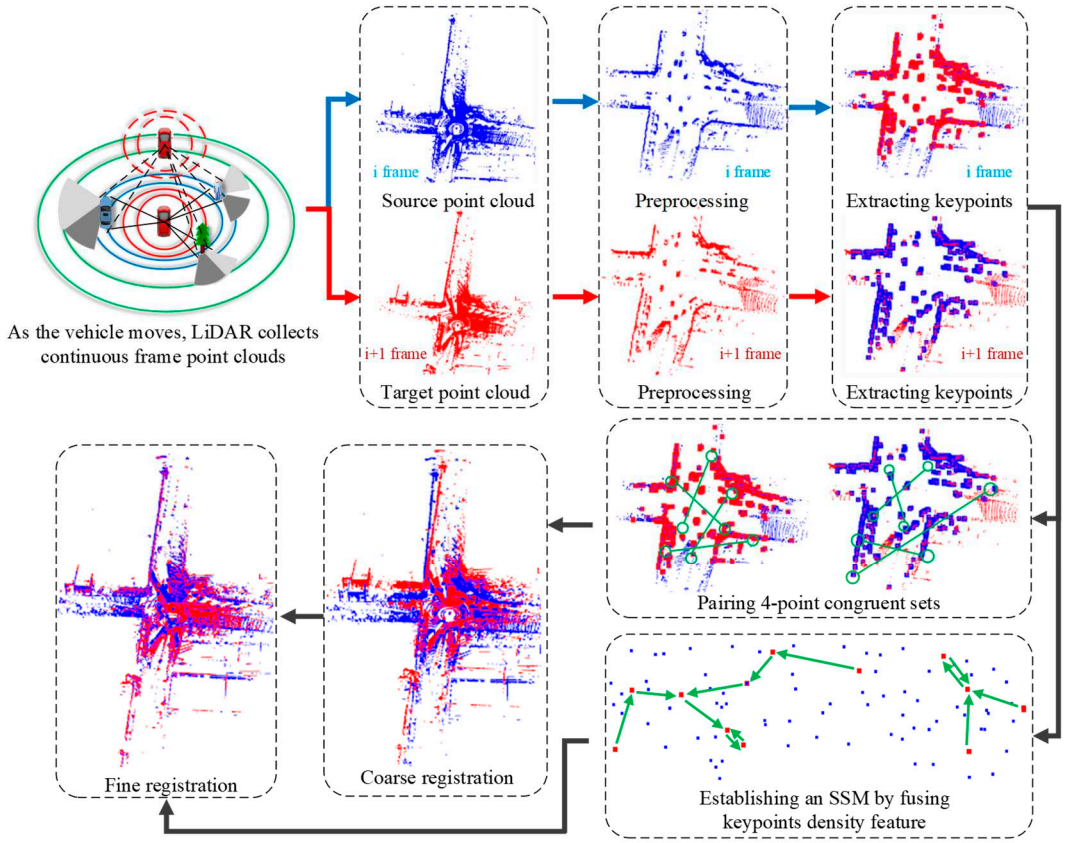

Figure 4. Architecture of the proposed method.

In the preprocessing, pass-through filter and improved voxel filter are used to trim and simplify the point cloud; In the coarse registration, ISS is used to extract the keypoints, and then 4PCS is used to provide the initial attitude; In the fine registration, the SSM model based on the density characteristics of key points is constructed, and the model is embedded in NDT to complete the fine registration.

3.1. Preprocessing

To reduce noise interference, the input point cloud is first preprocessed. For PCD scanned by Vehicular mounted LiDAR, there are many outliers and isolated noise points at the edges. The pass-through filter can be used to crop edges. In addition, voxel filtering can effectively simplify input point clouds, reduce subsequent calculations, and retain shape features.

Preprints (www.preprints.org) | NOT PEER-REVIEWED | Posted: 30 June 2023 doi:10.20944/preprints202306.2176.v1

The improved voxel filter limits the minimum number of points on the original basis, which means that the number of points in each voxel grid must reach the minimum limit value n_{min}, otherwise the size of voxel grids will be expanded. In addition, replace the voxel barycenter point P_b with the closest point P_v of the voxel barycenter:

$$P_b(x,y,z)=\left(\frac{1}{n}\sum_{i=1}^{n}x_i,\ \frac{1}{n}\sum_{i=1}^{n}y_i,\ \frac{1}{n}\sum_{i=1}^{n}z_i\right),\ n\geq n_{min} \tag{8}$$

$$P_v(x,y,z)=argmin_{(x_i,y_i,z_i)}\sqrt{(x_i-x_b)^2+(y_i-y_b)^2+(z_i-z_b)^2} \tag{9}$$

Where: n is the number of points in the voxel grid, (x_i, y_i, z_i) and (x_b, y_b, z_b) are the coordinates of any point P_i and the voxel barycenter point P_b in the grid, respectively.

The changes of the voxel filter are shown in Figure 5:

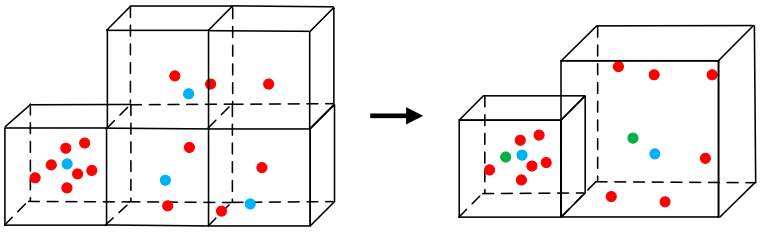

Figure 5. Schematic diagram of improved voxel filter (red dot is the origin points; blue dot is the voxel barycenter points; green dot is the closest point to the voxel barycenter).

Compared with before improvements, the grid size is larger at the sparse place, improving the Downsampling accuracy and reducing the number of edge outliers. To prevent data bias and ensure registration accuracy, the filtering result now uses the closest point to the barycenter instead of the barycenter itself.

3.1. I4PCS Coarse Registration

ISS [37] is an algorithm to describe the intrinsic shape characteristics of solid geometry, which can be used to extract keypoints from the point cloud. The idea of feature point detection is similar to Principal Component Analysis (PCA), which aims to reduce the dimensionality of high-dimensional data. The steps for ISS are as follows:

Step 1: Set the search radius r or the minimum number of neighboring points k for each point p_j (x_j, y_j, z_j) in point cloud P.

Step 2: Search for all points within radius r with p_j as the center, and calculate their weights W_{ji} based on the differences in the distribution of neighboring points. The value is:

$$W_{ji}=\frac{1}{||p_j-p_i||},\ |p_j-p_i|\leq r\cup i\leq k \tag{10}$$

Where: p_i is an anypoint in P

Step 3: Analyze the features within the neighborhood of point p_j, and calculate the covariance matrix cov $(p_j)$of each point p_j.

$$cov\left(p_j\right)=\sum_{|p_j-p_i|\leq r\cup i\leq k}W_{ji}(p_j-p_i)(p_j-p_i)^T\Big/\sum_{|p_j-p_i|\leq r\cup i\leq k}W_{ji} \tag{11}$$

Step 4: To establish a local reference frame (LRF), calculate the eigenvalues $\{\lambda_j^1, \lambda_j^2, \lambda_j^3\}$ and eigenvector $\{\vec{v_1},\vec{v_2},\vec{v_3}\}$ for each $cov(p_j)$. then, rank the eigenvalues in descending order. The established LRF is shown in Figure 6:

Step 5: To minimize the interference of diffusion points along the main direction on detection, non-maximum suppression (NMS) is applied to the salient features within r. Set threshold ε_1 and ε_2, Keypoints need to meet:

$$\lambda_j^2/\lambda_j^1\leq\varepsilon_1,\ \lambda_j^3/\lambda_j^2\leq\varepsilon_2,\ 0<\varepsilon_1,\varepsilon_2<1 \tag{12}$$

Step 6: Repeat the above steps until all points are traversed.

Preprints (www.preprints.org) | NOT PEER-REVIEWED | Posted: 30 June 2023 doi:10.20944/preprints202306.2176.v1

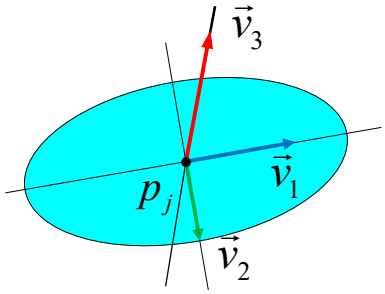

Figure 6. LRF of p_j.

ISS has low sensitivity to point cloud distribution and noise type, and has good stability; The accuracy of local feature description may not be as good as FPFH, but ISS is very efficient and suitable for real-time applications.

When the PCD is large, the process of searching similar sets and screening the best transformation matrix in 4PCS is slow and time-consuming. Most of the keypoints extracted by ISS are invariant to rotation, scale, and affine transformation, and retain local geometric features, which can be used as a stable and reliable initial point set for pairing. This point set can greatly improve the accuracy of the 4PCS algorithm in solving the optimal transformation. In addition, limiting the matching points to the keypoints set can greatly reduce the amount of calculation and make the coarse registration faster.

3.2. SSM-NDT Fine Registration

The traditional NDT algorithm uses PDF to solve the maximum possibility of surface shape coincidence of all blocks. When the local shape difference is large, the effect is poor, and the surface shape similarity should be improved first, so as to reduce the probability of matching dislocation caused by surface deviation.

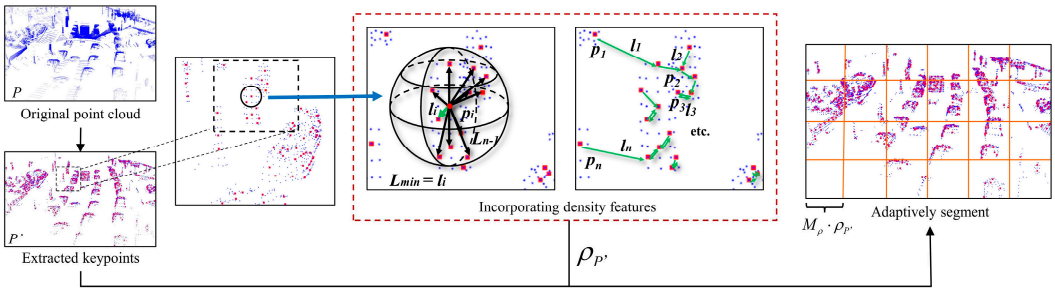

Figure 7. Fuse density features to construct SSM.

In addition, the size of the block directly affects the number of point clouds in the block, the distribution of point clouds and the total number of blocks, so setting a reasonable block size is a crucial step. To this end, a self-adaptive segmentation algorithm based on point cloud density features is proposed. Through this method, a segmentation model is constructed to cut the point cloud to cope with different distributions of PCD. The process of constructing a self-adaptive segmentation model is shown in Figure 7.

Let the Euclidean distance between any point p_i and other points in point cloud P be L, and the set of all L corresponding to p_i is $\xi_i = \{L_1, \ldots, L_{n-1}\}$. If all the elements in the set a are arranged in descending order, the minimum distance value l_i of p_i is:

$$l_i = min\left(L(p_i, q)\right),\ q=1,2,\ldots,n-1, q\neq p_i \tag{13}$$

Where: n is the number of points; q is any point that does not coincide with p_i.

Determining one L requires finding and computing n-1 Ls, which is extremely inefficient and unnecessary. By building a KD-tree to search, the calculation range is narrowed to around p_i. At this time, the density ρ_P of point cloud P is:

Preprints (www.preprints.org) | NOT PEER-REVIEWED | Posted: 30 June 2023 doi:10.20944/preprints202306.2176.v1

$$\rho_P = {}^{n}/_{\sum_{i=1}^{n} l_i} \tag{14}$$

To construct SSM based on point cloud density, a parameter that can adjust the block size is introduced: density multiple M_ρ. Embed the model in equation (7) to become F_{SSM}:

$$F_{SSM}(\vec{p}) = -\sum_{i=1}^{k_\rho} log f\left(T(\vec{p},\ \overrightarrow{R_k})\right),\quad k_\rho = {}^{V_{max}}/_{(M_\rho \cdot \rho_P)^3} \tag{15}$$

Where: k_ρ is the model quantity constructed in point cloud P; V_{max} is the volume of the maximum bounding box of point cloud P; R_k is the segmented point cloud block $\{r_1, ..., r_m\}$ under the k_ρ model quantity, r_m is a point within the block.

The pseudo program code for constructing an SSM is as follows.

Algorithm: constructing a Self-adaptive Segmentation Model

Input: Source point cloud $P = \{p_i\}$; threshold $\varepsilon_1, \varepsilon_2, \varepsilon_3$; Density multiple M_ρ
The search neighborhood K of the KD-tree;
Output: Space structure B and cells B_P

for $i \leftarrow 1$ to n
  for $j \leftarrow 1$ to K
    $W_{ji} \leftarrow 1 / |p_i - p_j|$
    $cov(p_i) \leftarrow \sum W_{ji}(p_j - p_i)(p_j - p_i)^T / \sum W_{ji}$
  end for
  $\{\lambda_j^1, \lambda_j^2, \lambda_j^3\} \leftarrow sort_{descending}(\text{eigenvalue}(cov(p_i)))$
  if $\lambda_j^2 / \lambda_j^1 \le \varepsilon_1$ and $\lambda_j^3 / \lambda_j^2 \le \varepsilon_2$
    add to $P' \leftarrow \{p'_1, \ldots, p'_n\}$
end for
for all points $p'_i \in P'$ do
  if $p'_j \ne p'_i$ and p'_j within K
    $L_j = |p'_j - p'_i| \leftarrow$ All points p'_j
    Corresponding point $p'_l \leftarrow l_n = L_{min}$
    sum(l) $\leftarrow$ all points p'_l
    $\rho_P = n$ / sum(l) $\leftarrow$ the number of p'_l
end for
Constructing spatial Structure B
Split B into cell set $B = \{B_1, \ldots, B_P\} \leftarrow$ the cell size $B_p = M_\rho \cdot \rho_P$,
for all points $p'_i \in P'$ do
  Find the cell B_p that contains p'_i
  Store p_i in B_p
end for

Additionally, the process of SSM-NDT is as follows:

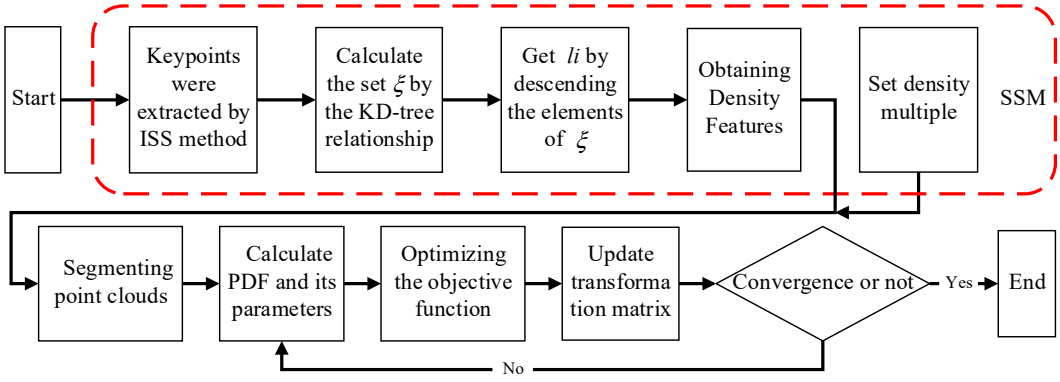

Preprints (www.preprints.org) | NOT PEER-REVIEWED | Posted: 30 June 2023 doi:10.20944/preprints202306.2176.v1

Figure 8. Flow chart of SSM-NDT.

SSM-NDT is an adaptive registration algorithm, which can produce accurate matching results in both dense and sparse regions, and has strong anti-interference. In PCD, each point is considered to carry information, and its relationship with nearby points determines whether the information is of high value. According to equation (14), the point cloud density is determined by the minimum distance l_i corresponding to all points. It can be inferred that there should be at least one point within the area with any point p_i as the center and l_i as the radius. If not, it means that the surrounding of the point is relatively sparse and the information load is low; On the contrary, it is dense and has a high probability of containing high-quality information. Therefore, if you want to improve the registration accuracy, you can put more point clouds in the same block, but this will increase the calculation time.

4. Experiment and Analysis

4.1. Experimental Environment

The experimental equipment is a laptop with a processor of Intel(R)Corei5-7300HQCPU@2.50GHz, 8GRAM, and a 64-bit Windows 10 operating system, the program runs in Visual Studio 2022+PCL (Point Cloud Library)1.12.0 [38]. The experiment verifies the effectiveness of the algorithm on the PandaSet dataset and The Real LiDAR-Derived PCD.

The comparison mainly includes registration accuracy, runtime, and anti-interference. Among them, *RMSE*, Deviation (*Dev*), Standard Deviation (*StDev*), and *Recall* were used as quantitative indicators for judging registration precision:

$$RMSE=\sqrt{\frac{1}{n}\sum_{i=1}^{n}(x_i-y_i)^2},\ (1<i<N) \tag{16}$$

$$Dev=\frac{1}{n}\sum_{i=1}^{n}(x_i-y_i),\ (1<i<N) \tag{17}$$

$$StDev=\sqrt{\frac{1}{n}\sum_{i=1}^{n}(x_i-\bar{x})},\ (1<i<N) \tag{18}$$

$$Recall=\frac{TP}{TP+FN} \tag{19}$$

Where: n is the number of point-pairs; N is the number of points; x_i and y_i are a point-pair; $\bar{x}$ is the mean of x_i; *TP* (True Positive) is the number of correctly matched point-pairs; *FN* (False Negative) is the number of incorrectly matched point-pairs.

Specifically, RMSE describes the accuracy of the algorithm for real-world transformations; Dev measures the partial accuracy and stability of the algorithm; The smaller StDev, the more consistent and accurate the calculation results; Recall measures the ability of the algorithm to correctly match point-pairs.

4.2. Parameter Settings

The influence of parameter values on the method cannot be underestimated. The rules for setting parameters in ISS can be referred to reference [24], the effects of voxel grid size R_s and density multiple M_ρ on the performance of SSM-NDT are shown in Figure 9.

Preprints (www.preprints.org) | NOT PEER-REVIEWED | Posted: 30 June 2023 doi:10.20944/preprints202306.2176.v1

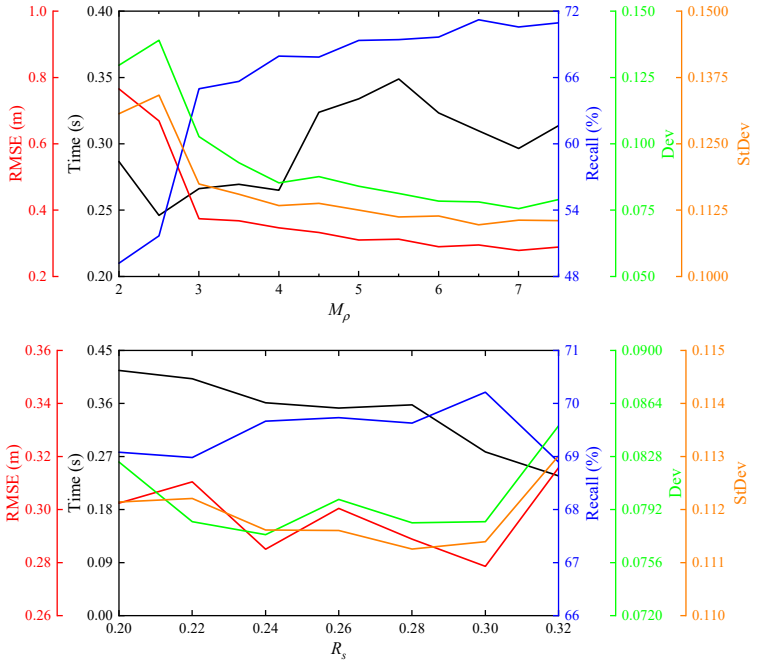

Figure 9. The impact of different R_s and M_ρ on registration results.

As shown in Figure 9, the M_ρ value is positively correlated with registration accuracy. At M_ρ= 3, RMSE, Dev, and StDev rapidly decrease around, and then remain stable; The M_ρ value and running time show a "W" shape with low left and high right. The R_s value has a negative correlation with the running time; RMSE, Dev, and StDev show a "W" or "V" shaped trend as Rs increase, while the recall rate shows an inverted "U" shape.

F_{SSM} varies with M_ρ and ρ_P for different PCDs. Since the change in ρ_P between two frames is small, M_ρ becomes the most important dependent variable. According to equation (15), if M_ρ decreases, k_ρ increases, and r_m decreases. This means that the number of points in each block will decrease, while the total number of blocks increases. Although this can reduce the number of $f(\vec{x})$, it cannot contain enough surface shape features, and the accuracy will decrease; if M_ρ is too large, the calculation amount of each $f(\vec{x})$ will increase, more feature information can be included, and the accuracy will increase, but the running time will increase sharply. The parameters set for the experiment are shown in Table 1.

Table 1. Method's parameter set.

parameter	PandaSet	The Real LiDAR-Derived PCD	explain
R_s	0.3	0.15	Voxel grid size
n_{min}	2	2	Minimum number of points in the grid
r	0.4	0.3	ISS search radius
r_{NMS}	0.4	0.3	NMS radius
ε_1	0.8	0.7	The ratio of the second eigenvalue to the first eigenvalue
ε_2	0.6	0.5	The ratio of the third eigenvalue to the second eigenvalue
k	6	4	Number of ISS search points
O_r	0.35	0.35	Approximate overlap rate
D_t	0.4	0.4	Target distance
ε	0.4	0.4	Distance threshold of point-pairs
M_ρ	6	5	Density multiple

4.3. *PandaSet Dataset*

PandaSet, an open-source commercial dataset, is collected by a forward 128-line MEMS LiDAR (PandarGT) and a mechanically rotated 64-line LiDAR (Pandar64). This dataset covers the most

Preprints (www.preprints.org) | NOT PEER-REVIEWED | Posted: 30 June 2023 doi:10.20944/preprints202306.2176.v1

challenging driving conditions in L5 autonomous driving, including complex urban environments, dense traffic and pedestrians, steep hills, buildings, and lighting conditions at different times.

4.3.1. Accuracy

Three scenes are randomly selected and two frames are selected from each scene. Our method was compared with ICP, GICP, NDT, NDT+ICP, In Ref. [30] algorithm, and In Ref. [31] algorithm. The registration effects are shown in Figure 10.

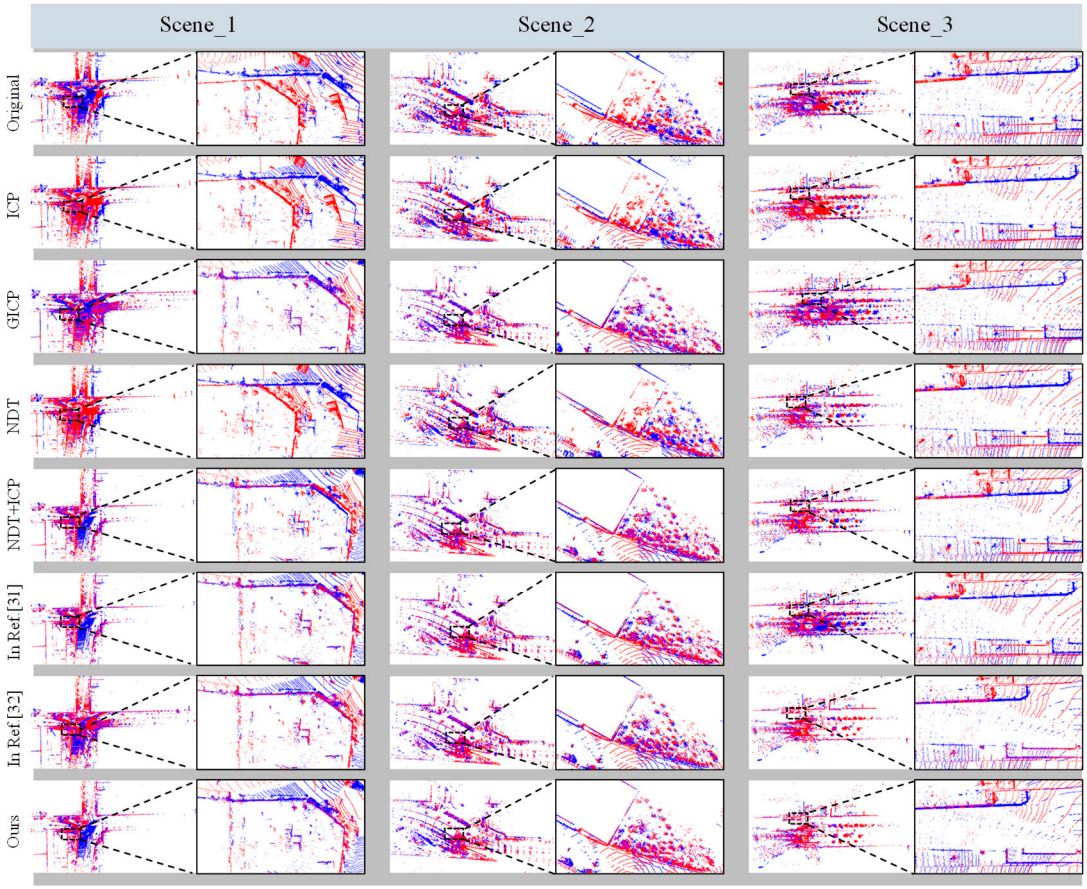

Figure 10. Visual comparison diagram of various algorithms.

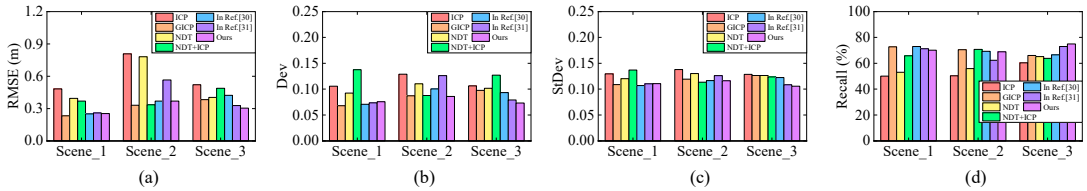

Figure 11. Registration accuracy comparison chart.

Different from Scene_1 and Scene_2, the shapes of buildings on both sides of the road in Scene_3 are similar, the corners of buildings are fewer, and there are many pedestrians. These characteristics mean that the surface features of the point cloud are not obvious, there are many noises, and the matching distance is large, etc., which makes the registration difficulty of Scene_3 significantly higher than others.ICP and NDT only reduce a small part of the rotation error, and the translation error is still very large. GICP, NDT+ICP, and In Ref. [30] can only reduce the error under Scene_1 and Scene_2. Only In Ref. [31] and Ours reduce the error in all scenes. In the enlarged figures of Scene_2 and Scene_3, it is shown that the overlap degree of In Ref. [31] is lower than Ours.

Most of the above algorithms rely on parameter settings, and improper parameter settings may lead to the algorithm falling into local optima. For more objectivity, each method was repeated 500 times. Figure 11 shows the comparison of the mean values of RMSE, Dev, StDev, and Recall. The indicators of Ours in the three scenes rank high, and there is a small gap with the optimal method.

Preprints (www.preprints.org) | NOT PEER-REVIEWED | Posted: 30 June 2023 doi:10.20944/preprints202306.2176.v1

Especially in Scene_ 3, Ours is not only the smallest on RMSE, Dev, and STDev, and also the largest on recall.

4.3.2. Time

For practical application scenarios, the registration time between two frames is a very important indicator. Table 2 lists the running time of each method and whether they are successfully registered (SR).

Table 2. Running time of algorithms time (s).

Algorithm	Scene_1 (*N*=169171)			Scene_2 (*N*=148700)			Scene_3 (*N*=178386)		
	Mean	**Max**	**SR**	**Mean**	**Max**	**SR**	**Mean**	**Max**	**SR**
ICP	3.3359	6.4430		8.0936	20.1930		1.3636	**1.9920**	
GICP	7.9151	9.203	✓	12.1920	19.727	✓	4.7985	6.599	
4PCS	1.7380	2.7320		1.5456	2.3110		1.7394	2.8950	
NDT	15.6830	21.2550		18.2558	19.2390		19.4366	26.1480	
NDT+ICP	5.7949	8.2260	✓	3.3800	3.7620	✓	12.6595	16.1310	
In Ref. [30]	5.1405	5.7990	✓	3.4190	3.9030	✓	7.1740	11.6440	
In Ref. [31]	2.5198	3.5090	✓	2.1809	3.1740	✓	2.5098	3.7270	✓
Ours	**0.6894**	**2.3970**	✓	**0.5645**	**2.0360**	✓	**0.5707**	2.8350	✓

According to the data in Table 2, ICP, 4pcs, and NDT failed all registration. ICP is sensitive to the initial position and fails when the point-to-point distance is large; 4pcs does not need iteration and its running time is very short; NDT takes abnormal time to match when the point cloud density distribution is uneven.

GICP, NDT+ICP, and In Ref. [30] were successfully registered in Scene_1 and Scene_2. GICP constructs the cost function through the covariance matrix of the surface based on ICP, which improves the success rate but takes more time; NDT+ICP simplifies the point cloud through the voxel filter, which greatly reduces the time; the average time of the method in In Ref. [30] is the same as that of NDT+ICP is similar, and its registration is better as shown in Figure 9. In Scene_3, only the In Ref. [31] and Ours are successfully registered. Ours takes at least 70%-80% less time in all scenarios than others. Therefore, the method in this paper has great advantages in efficiency, while taking into account the accuracy.

4.3.3 Stability

4PCS is similar to the RANSAC framework, which is uncertain, and it is necessary to improve stability. By matching different coarse and fine registrations, we had explored the influence of I4PCS and SSM-NDT on the stability respectively. The results of 500 experiments are arranged in ascending order, and the changes are shown in Figure 12.

According to the change of the RMSE curve, I4PCS+ICP tends to the lower right corner than 4PCS+ICP, which indicates that I4PCS can effectively reduce the frequency and amplitude of anomalies than 4PCS. Similarly, the comparison between I4PCS+NDT and I4PCS+SSM-NDT shows that introducing SSM into NDT can effectively reduce instability. According to the change of the time curve, I4PCS+ICP and 4PCS+ICP approximately overlap, indicating that their efficiency is not much different; while 4PCS+KDF-NDT only slightly increases at the end, indicating that KDF-NDT takes less time and reduces fluctuations.

Preprints (www.preprints.org) | NOT PEER-REVIEWED | Posted: 30 June 2023 doi:10.20944/preprints202306.2176.v1

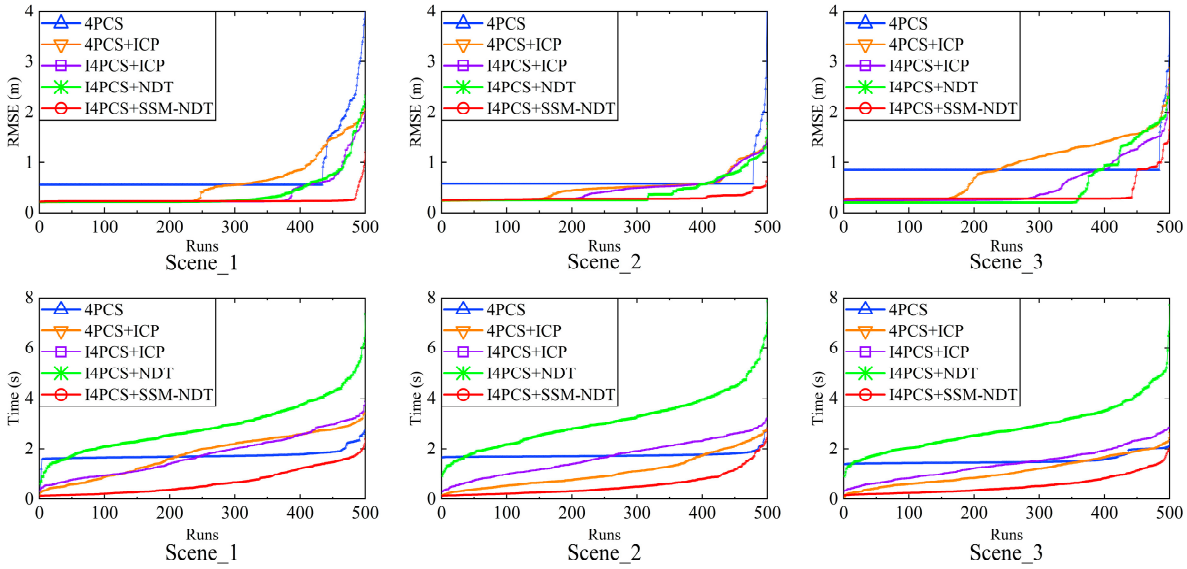

Figure 12. Fluctuations in Results of Different Schemes (Arrange the results of 500 experiments in ascending order).

The analysis shows that I4PCS and SSM-NDT mainly improve accuracy and efficiency respectively, and both improve the stability together. In Scene_2 and Scene_3, although the introduction of ISS as a pre-step will increase the time-consuming of rough registration, it can reduce the calculation amount of fine registration and shorten the overall time; SSM-NDT can correct the abnormality of coarse registration in time.

3.3.4. Anti-Interference

During the outdoor scanning process of LiDAR, it is inevitable that the collected data will be interfered with. Thus, anti-interference is one of the important indicators to evaluate the quality of the method. To verify the anti-interference ability of the method, the following four types of interference (IF) are added to Scene_1:

1. Remove 10% of the local point cloud (IF1): there are obstructions or the light intensity is very weak.
2. Remove 20% of the global point cloud (IF2): under the influence of bad weather, data loss may occur.
3. Add 20% local noise (IF3): strong reflection may occur on the surface with large curvature.
4. Add 50% global noise (IF4): beams of different lidars may interfere with each other.

The PCD after interference is shown in Figure 13, and the anti-interference ability of the method is quantitatively evaluated by the relative error (RE). The relative error distribution of each index is shown in Figure 14.

$$RE = \left| IF_{After} - IF_{Before} \right| / IF_{Before} \times 100\% \tag{20}$$

Where: IF_{Before} and IF_{After} are the values before and after the interference respectively.

The relative accuracy error of most algorithms is smaller in IF2 and IF4 than in IF1 and IF3, and the time error is smaller in IF3 and IF4. In terms of accuracy, the error of the method in this paper is small among the four types of disturbances; in terms of time, the data in Table 2 shows that the algorithm in this paper takes a very short time, although the error performance is average, and the absolute value of the error is less than 0.2s.

Preprints (www.preprints.org) | NOT PEER-REVIEWED | Posted: 30 June 2023 doi:10.20944/preprints202306.2176.v1

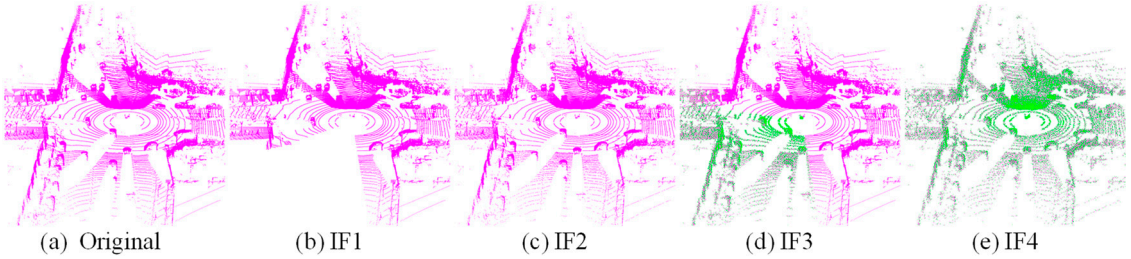

Figure 13. The image after adding four kinds of interference to Scene_1 (purple is the origin cloud; green is the Gaussian noise added).

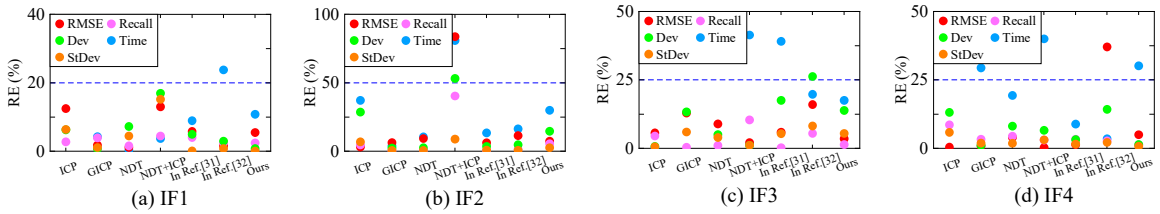

Figure 14. Scatter plot of relative error of each algorithm before and after four types of interference.

Different methods exhibit different immunity to different disturbances. Ours can be anti-interference in the coarse and fine registration. ISS is more inclined to areas with high curvature and high features, while noise is usually not in this area; SSM incorporates a large number of surface features to reduce the influence of local area anomalies.

4.4. The Real LiDAR-Derived PCD

To further verify the effectiveness and applicability, we had tested the real PCD collected by forward MEMS LiDAR (RS-LiDAR M1, RoboSense, Shenzhen, China). The PCD perspective is relatively small and there are few matching targets. Figure 14 and Table 3 show the registration results on this PCD.

In the Library scene, the offset between two frames is small, and most of the methods can be registered successfully. The Mean Time of Ours is only 0.32s, which is at least 60% higher than other methods. The rotation offset between two frames in the Car scene is large, and only NDT+ICP and Ours are successful. The accuracy of Ours is higher, and the time is only 0.84s, which is 65.5% higher than that of NDT+ICP. Therefore, the algorithm in this paper has great advantages in similar scenarios.

Internal factors that affect time include algorithm principles and initial values; external factors are related to PCD. The algorithm in this paper is efficient and concise. Firstly, the improved voxel filtering simplifies PCD; secondly, I4PCS does not need iteration and is highly efficient; finally, SSM-NDT automatically determines the optimal segmentation size to further improve efficiency. Therefore, in each experimental scenario, the mean time consumption of this algorithm is significantly less than that of others, and the efficiency is far ahead.

Preprints (www.preprints.org) | NOT PEER-REVIEWED | Posted: 30 June 2023 doi:10.20944/preprints202306.2176.v1

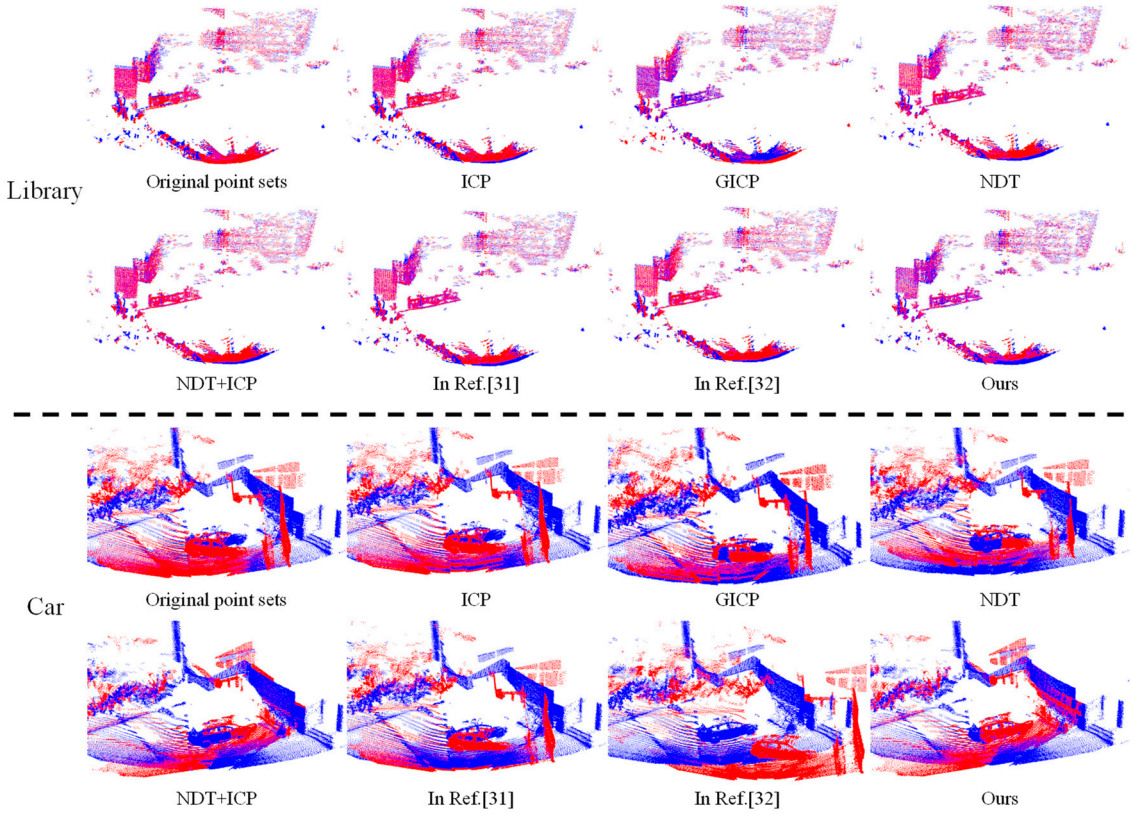

Figure 15. Registration results of The Real LiDAR-Derived PCD.

Table 3. Comparison of evaluation indicators for registration results of The Real LiDAR-Derived PCD.

Algorithm	Mean RMSE	Mean Dev	Mean StDev	Mean Recall	Mean Time	Max Time	SR
Library(*N*=50215)							
ICP	0.2240	0.1136	0.1391	**67.4818**	4.3752	5.1180	✓
GICP	**0.1672**	0.0717	0.1118	65.8270	2.1092	5.201	✓
4PCS	0.4744	0.0896	0.1137	56.2409	1.5248	2.5150	
NDT	0.1707	**0.0711**	**0.1116**	64.6528	8.0606	9.7360	✓
NDT+ICP	0.1690	0.0722	0.1131	66.6853	3.2195	3.5250	✓
In Ref. [30]	0.1677	0.0738	**0.1116**	64.9547	1.5812	1.8710	✓
In Ref. [31]	0.2008	0.0895	0.1139	66.9021	0.8389	**1.4030**	✓
Ours	0.1736	0.0731	0.1135	65.4235	**0.3276**	3.5640	✓
Car(*N*=72770)							
ICP	0.1351	0.0858	0.1268	64.9637	1.2060	**1.3260**	
GICP	0.1290	0.0773	0.11644	64.2627	1.6893	2.149	
4PCS	0.1771	0.0932	0.1267	63.3158	2.6987	6.0140	
NDT	0.1311	0.1122	0.1357	56.5143	12.7207	13.8180	
NDT+ICP	0.1268	0.0741	0.1051	**76.9665**	2.4270	2.9370	✓
In Ref. [30]	0.2071	0.0910	0.1165	66.2869	1.4699	3.1430	
In Ref. [31]	0.4013	0.1455	0.1347	44.4968	1.3607	2.0880	
Ours	**0.1244**	**0.0546**	**0.0962**	72.2800	**0.8414**	5.1380	✓

Preprints (www.preprints.org) | NOT PEER-REVIEWED | Posted: 30 June 2023 doi:10.20944/preprints202306.2176.v1

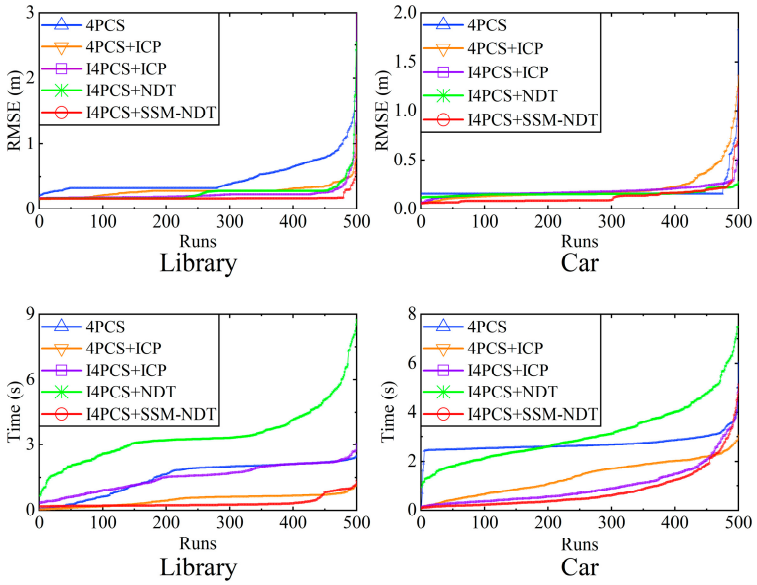

Figure 16. Registration changes of The Real LiDAR-Derived PCD.

In the car scene stability test results, unexpectedly, the change of the end segment of the I4PCS+SSM-NDT curve is roughly the same as that of other algorithms, indicating that the possibility of errors has not been reduced. It is speculated that the continuity between the two frames of the scene is insufficient and the overlap is too small.

5. Conclusion and Outlook

A fast registration method based on MEMS lidar target point cloud is proposed. The method uses a pass-through filter and voxel filter with minimum points number to preprocess; Using the keypoints of ISS as two input point clouds, 4PCS effectively obtains the initial transformation matrix; In the precise registration process, the density feature information of keypoints is used to create the SSM to retrofit the NDT. This method is called SSM-NDT. Considering the distribution characteristics of different point clouds, SSM-NDT solves the problems of poor applicability and low efficiency of traditional NDT algorithm.

Experiments were carried out in PandaSet and The Real LiDAR-Derived PCD, the results show that when the registration accuracy is similar, the registration time is significantly reduced compared with other methods, and the improvement is more than 60%. In addition, it also shows anti-interference in a variety of abnormal conditions.

One limitation of the proposed algorithm is that if the scene continuity is very low, the probability of abnormal registration cannot be reduced. To overcome this limitation, in future research, we plan to consider the surface smoothness and connectivity of point clouds in the registration process to optimize the accuracy of fast alignment when the overlap is low.

Author Contributions: Conceptualization, B.L. and X.L; methodology, B.L; project administration, X.L.; software, B.L.; validation, B.L. and M.L.; resources, C.L.; datacuration, B.L.; writing—original draft preparation, B.L. and S.L; writing—review and editing, B.L., X.L. and S.L.; visualization, B.L.; supervision, X.L. and M.L.; funding acquisition, X.L. All authors have read and agreed to the published version of the manuscript.

Funding: This paper is partly supported by the Natural Science Foundation of Jilin Province under grant YDZJ202201ZYTS655.

Data Availability Statement: The PandaSet dataset is available at https://scale.com/resources/download/pandaset. The Real LiDAR-Derived PCD are available to readers by contacting the corresponding author.

Acknowledgments: The authors thank the Mechanical and Control Engineering 219 Lab of Baicheng Normal University.

Conflicts of Interest: The authors declare no conflict of interest.

Reference

1. Shao, H.; Zhang, Z.; Feng, X.; Zeng, D. SCRnet: A Spatial Consistency Guided Network Using Contrastive Learning for Point Cloud Registration. *Symmetry* **2022**, *14*. [CrossRef]
2. Li, X.; Mo, S.; Huang, H.; Yang, S. Multi-source point cloud registration method based on automatically calculating overlap. Infrared and Laser Engineering **2021**, *50*, 270-278,8. [CrossRef]
3. Besl, P.J.; McKay, N.D. A method for registration of 3-D shapes. *IEEE Transactions on Pattern Analysis and Machine Intelligence* **1992**, *14*, 239-256. [CrossRef]
4. Chen, Y.; Medioni, G. Object modeling by registration of multiple range images. In Proceedings of the Proceedings. 1991 IEEE International Conference on Robotics and Automation, 9-11 April 1991, 1991; pp. 2724-2729 vol.2723. [CrossRef]
5. Segal, A.; Hähnel, D.; Thrun, S. *Generalized-ICP*; 2009. [CrossRef]
6. Chetverikov, D.; Stepanov, D.; Krsek, P. Robust Euclidean alignment of 3D point sets: the trimmed iterative closest point algorithm. *Image and Vision Computing* **2005**, *23*, 299-309. [CrossRef]
7. Serafin, J.; Grisetti, G. NICP: Dense normal based point cloud registration. In Proceedings of the 2015 IEEE/RSJ International Conference on Intelligent Robots and Systems (IROS), 28 Sept.-2 Oct. 2015, 2015; pp. 742-749. [CrossRef]
8. Bae, K.-H.; Lichti, D.D. A method for automated registration of unorganised point clouds. *ISPRS Journal of Photogrammetry and Remote Sensing* **2008**, *63*, 36-54. [CrossRef]
9. Wang, X.; Li, Y.; Peng, Y.; Ying, S. A Coarse-to-Fine Generalized-ICP Algorithm With Trimmed Strategy. *IEEE Access* **2020**, *8*, 40692-40703. [CrossRef]
10. Zhang, J.; Yao, Y.; Deng, B. Fast and Robust Iterative Closest Point. *IEEE Trans Pattern Anal Mach Intell* **2022**, *44*, 3450-3466. [CrossRef]
11. Magnusson, M.; Lilienthal, A.; Duckett, T. Scan registration for autonomous mining vehicles using 3D-NDT. *Journal of Field Robotics* **2007**, *24*, 803-827. [CrossRef]
12. Aiger, D.; Mitra, N.J.; Cohen-Or, D. 4-points congruent sets for robust pairwise surface registration. *ACM Transactions on Graphics* **2008**, *27*, 1-10. [CrossRef]
13. Theiler, P.W.; Wegner, J.D.; Schindler, K. Keypoint-based 4-Points Congruent Sets – Automated marker-less registration of laser scans. *ISPRS Journal of Photogrammetry and Remote Sensing* **2014**, *96*, 149-163. [CrossRef]
14. Sipiran, I.; Bustos, B. *A Robust 3D Interest Points Detector Based on Harris Operator*; 2010; pp. 7-14. [CrossRef]
15. Lowe, D.G. Object recognition from local scale-invariant features. In Proceedings of the Proceedings of the Seventh IEEE International Conference on Computer Vision, 20-27 Sept. 1999, 1999; pp. 1150-1157 vol.1152. [CrossRef]
16. Xu, Y.; Boerner, R.; Yao, W.; Hoegner, L.; Stilla, U. Pairwise coarse registration of point clouds in urban scenes using voxel-based 4-planes congruent sets. *ISPRS Journal of Photogrammetry and Remote Sensing* **2019**, *151*, 106-123. [CrossRef]
17. Rusu, R.B.; Blodow, N.; Marton, Z.C.; Beetz, M. Aligning point cloud views using persistent feature histograms. In Proceedings of the 2008 IEEE/RSJ International Conference on Intelligent Robots and Systems, 22-26 Sept. 2008, 2008; pp. 3384-3391. [CrossRef]
18. Rusu, R.B.; Blodow, N.; Beetz, M. Fast Point Feature Histograms (FPFH) for 3D registration. In Proceedings of the 2009 IEEE International Conference on Robotics and Automation, 12-17 May 2009, 2009; pp. 3212-3217. [CrossRef]
19. Salti, S.; Tombari, F.; Di Stefano, L. SHOT: Unique signatures of histograms for surface and texture description. *Computer Vision and Image Understanding* **2014**, *125*, 251-264. [CrossRef]
20. Frome, A.; Huber, D.; Kolluri, R.; Bülow, T.; Malik, J. Recognizing Objects in Range Data Using Regional Point Descriptors. In Proceedings of the Computer Vision - ECCV 2004, Berlin, Heidelberg, 2004//, 2004; pp. 224-237. [CrossRef]
21. Li, M.; Hashimoto, K. Curve Set Feature-Based Robust and Fast Pose Estimation Algorithm. *Sensors (Basel)* **2017**, *17*. [CrossRef]
22. Tao, W.; Hua, X.; Chen, Z.; Tian, P. Fast and Automatic Registration of Terrestrial Point Clouds Using 2D Line Features. *Remote Sensing* **2020**, *12*. [CrossRef]
23. Yue, X.; Liu, Z.; Zhu, J.; Gao, X.; Yang, B.; Tian, Y. Coarse-fine point cloud registration based on local point-

pair features and the iterative closest point algorithm. *Applied Intelligence* **2022**, *52*, 12569-12583. [CrossRef]
24. Zhang, X.; Gao, R.; Sun, Q.; Cheng, J. An Automated Rectification Method for Unmanned Aerial Vehicle LiDAR Point Cloud Data Based on Laser Intensity. *Remote Sensing* **2019**, *11*. [CrossRef]
25. Prokop, M.; Shaikh, S.A.; Kim, K.-S. Low Overlapping Point Cloud Registration Using Line Features Detection. *Remote Sensing* **2019**, *12*. [CrossRef]
26. Chen, S.; Nan, L.; Xia, R.; Zhao, J.; Wonka, P. PLADE: A Plane-Based Descriptor for Point Cloud Registration With Small Overlap. *IEEE Transactions on Geoscience and Remote Sensing* **2020**, *58*, 2530-2540. [CrossRef]
27. Wang, J.; Wang, P.; Li, B.; Fu, R.; Zhao, S.; Zhang, H. Discriminative optimization algorithm with global–local feature for LIDAR point cloud registration. *International Journal of Remote Sensing* **2021**, *42*, 9003-9023. [CrossRef]
28. Yang, J.; Luo, W.; Zhang, Y.; Chang, B.; Zheng, R.; Wu, M.; Shao, X. Establishment of a Coal Mine Roadway Model Based on Point Cloud Feature Matching. *Mathematical Problems in Engineering* **2022**, *2022*, 1-14. [CrossRef]
29. Yang, J.; Wang, C.; Luo, W.; Zhang, Y.; Chang, B.; Wu, M. Research on Point Cloud Registering Method of Tunneling Roadway Based on 3D NDT-ICP Algorithm. *Sensors (Basel)* **2021**, *21*. [CrossRef]
30. Xu, G.; Pang, Y.; Bai, Z.; Wang, Y.; Lu, Z. A Fast Point Clouds Registration Algorithm for Laser Scanners. *Applied Sciences* **2021**, *11*. [CrossRef]
31. Baek, J.; Park, J.; Cho, S.; Lee, C. 3D Global Localization in the Underground Mine Environment Using Mobile LiDAR Mapping and Point Cloud Registration. *Sensors (Basel)* **2022**, *22*. [CrossRef]
32. Wu, B.; Yang, L.; Wu, Q.; Zhao, Y.; Pan, Z.; Xiao, T.; Zhang, J.; Wu, J.; Yu, B. A Stepwise Minimum Spanning Tree Matching Method for Registering Vehicle-Borne and Backpack LiDAR Point Clouds. *IEEE Transactions on Geoscience and Remote Sensing* **2022**, *60*, 1-13. [CrossRef]
33. Wang, H.; Liang, H.; Li, Z.; Zhou, P.; Chen, L. A fast coarse-to-fine point cloud registration based on optical flow for autonomous vehicles. *Applied Intelligence* **2023**. [CrossRef]
34. Li, J.; Zhan, J.; Zhou, T.; Bento, V.A.; Wang, Q. Point cloud registration and localization based on voxel plane features. *ISPRS Journal of Photogrammetry and Remote Sensing* **2022**, *188*, 363-379. [CrossRef]
35. Théodose, R.; Denis, D.; Chateau, T.; Fremont, V.; Checchin, P. A Deep Learning Approach for LiDAR Resolution-Agnostic Object Detection. *IEEE Transactions on Intelligent Transportation Systems* **2022**, *23*, 14582-14593. [CrossRef]
36. Biber, P.; Strasser, W. The normal distributions transform: a new approach to laser scan matching. In Proceedings of the Proceedings 2003 IEEE/RSJ International Conference on Intelligent Robots and Systems (IROS 2003) (Cat. No.03CH37453), 27-31 Oct. 2003, 2003; pp. 2743-2748 vol.2743. [CrossRef]
37. Zhong, Y. Intrinsic shape signatures: A shape descriptor for 3D object recognition. In Proceedings of the 2009 IEEE 12th International Conference on Computer Vision Workshops, ICCV Workshops, 2009; pp. 689-696. [CrossRef]
38. Munaro, M.; Rusu, R.B.; Menegatti, E. 3D robot perception with Point Cloud Library. *Robotics and Autonomous Systems* **2016**, *78*, 97-99. [CrossRef]